ATP-independent reversal of a membrane protein aggregate by a chloroplast SRP

Peera Jaru-Ampornpan[1], Kuang Shen[1,3], Vinh Q. Lam[1,3], Mona Ali[2], Sebastian Doniach[2], Tony Z. Jia[1], Shu-ou Shan[1]

Supplementary information contains:

Supplementary Figures 1-7

Supplementary Table 1

Supplementary Note

Nature Structural & Molecular Biology: doi:10.1038/nsmb.1836

Supplementary Figure 1

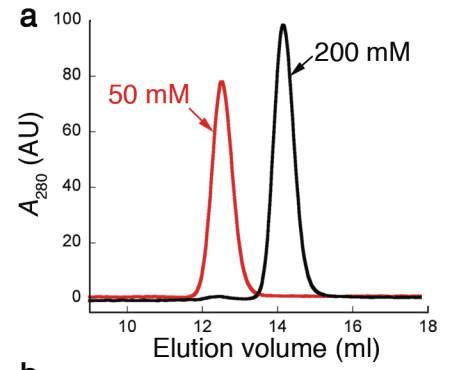

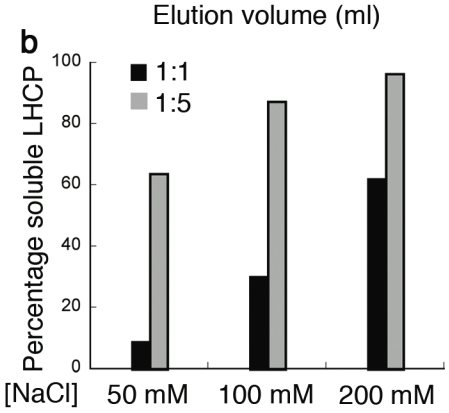

c

[NaCl] mM	K_d (nM)
50	580
100	325
200	108
300	143

cpSRP43 is active at higher ionic strength, but is present as inactive multimeric forms at lower ionic strength. (**a**) cpSRP43 runs as a monomer on Superdex 200 in buffer containing 200 mM NaCl (black trace), but exhibits aberrant mobility in buffer containing 50 mM NaCl (red trace). (**b**) The amount of solubilized LHCP (1 μM) at equilibrium in the presence of 1 μM (black) or 5 μM (gray) cpSRP43 in buffer with different salt concentrations. (**c**) List of the K_d values for the LHCP-cpSRP43 interaction, determined by fluorescence anisotropy, at different salt concentrations.

Supplementary Figure 2

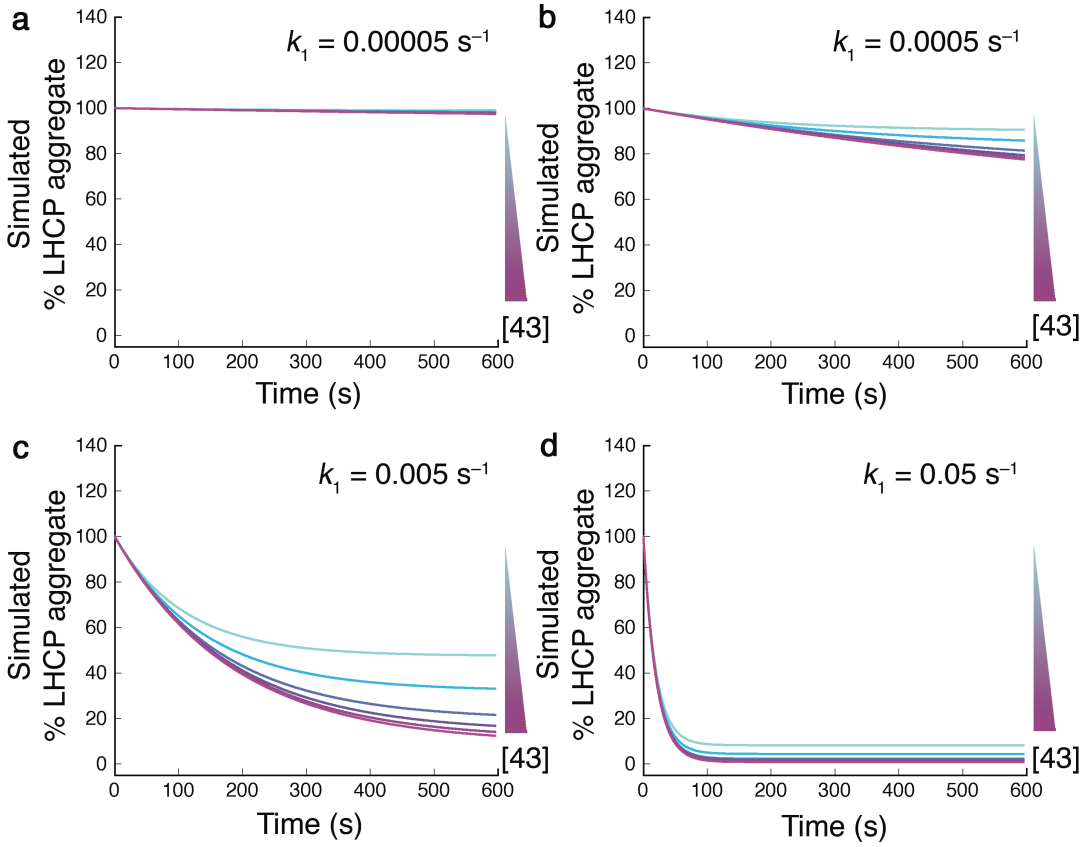

Kinetic simulations based on the passive mechanism in Figure 4c, which showed that the rates of disaggregation are independent of cpSRP43 concentration when the rates of spontaneous disaggregation (k_1) were varied over the range of 0.00005 – 0.05 s^{-1}.

Supplementary Figure 3

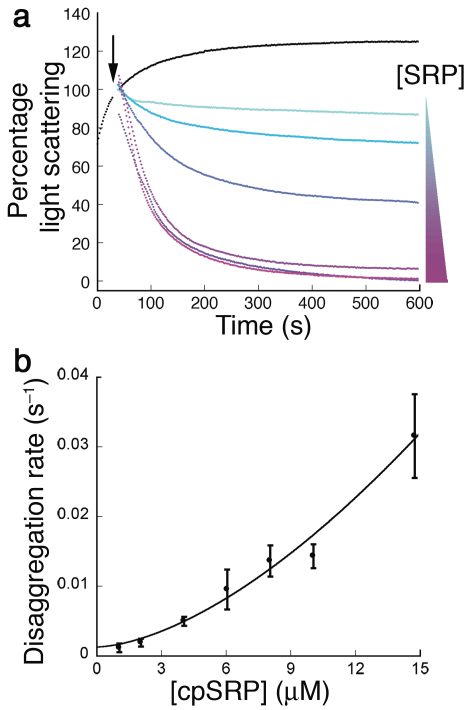

cpSRP actively reversed LHCP aggregation. (**a**) Time courses for disaggregation of LHCP (1 μM) at varying concentrations (2 – 10 μM) of cpSRP. The black arrow marks the time of cpSRP addition. (**b**) Concentration dependence of the forward rate constants of disaggregation reactions (k_f; see text for derivation). The fits to equation **3** in Methods gave a Hill coefficient of 1.7.

Supplementary Figure 4

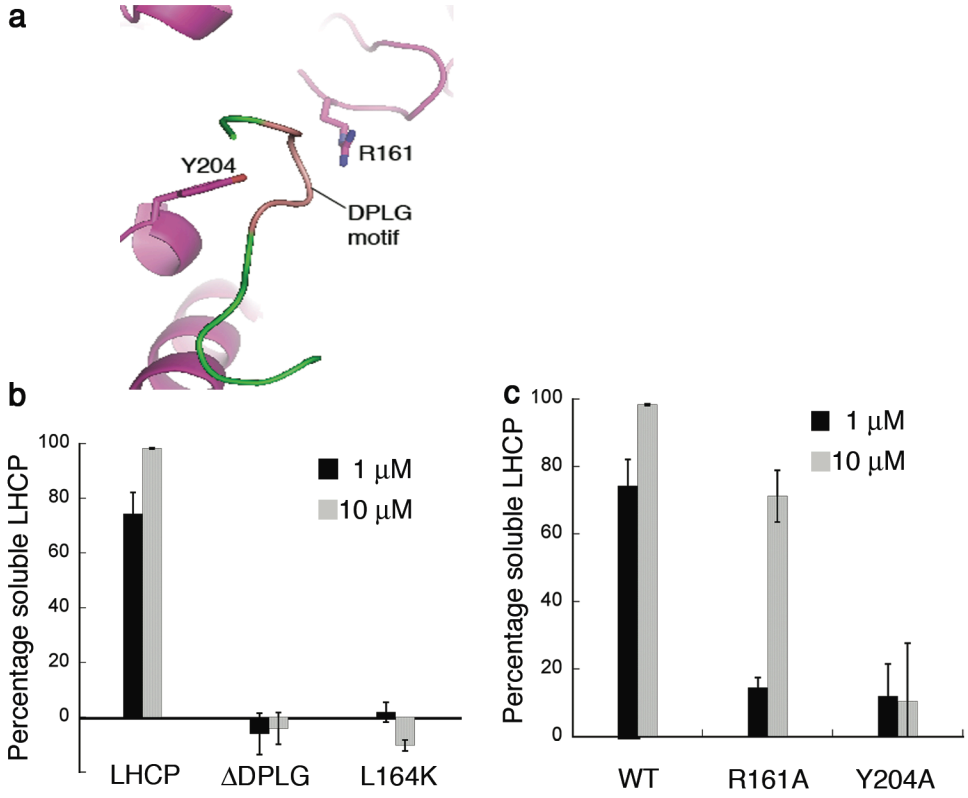

Specific binding interactions between the L18 motif of LHCP and cpSRP are essential for chaperone activity. (**a**) The crystal structure of the L18 peptide (green) bound to the CD1–Ank4 fragment of cpSRP43 (magenta)[19]. The DPLG motif is highlighted in pink. The two residues from cpSRP43 that make important contacts to this motif, R161 and Y204, are shown in sticks. (**b**) The amount of soluble LHCP (1 μM) or its mutants, ΔDPLG and L164K, at equilibrium in the presence of 1 μM (black) or 10 μM (gray) cpSRP. (**c**) The amount of soluble LHCP (1 μM) at equilibrium in the presence of 1 μM (black) or 10 μM (gray) cpSRP or its mutants, cpSRP-R161A and cpSRP-Y204A.

Supplementary Figure 5

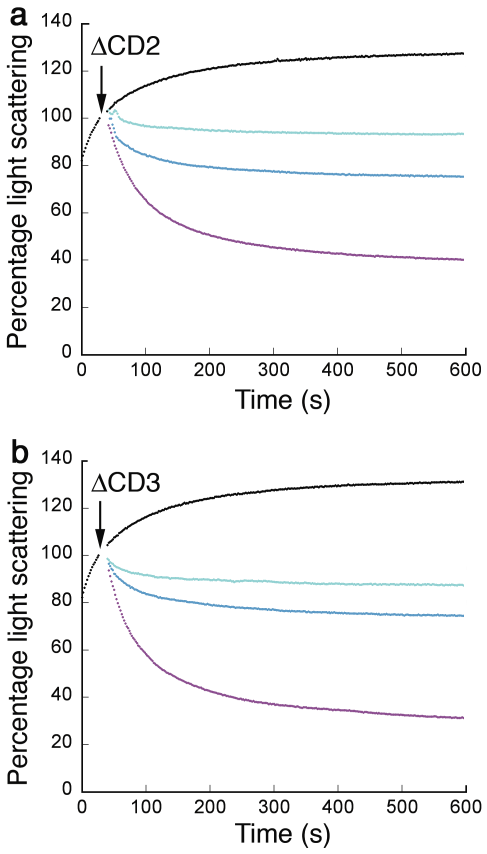

cpSRP43 deletion mutants, ΔCD2 and ΔCD3, can efficiently reverse LHCP aggregation. Time courses for disaggregation reactions by 2 μM (cyan), 4 μM (blue) and 8 μM (magenta) of cpSRP43 ΔCD2 (**a**) and cpSRP43 ΔCD3 (**b**).

Supplementary Figure 6

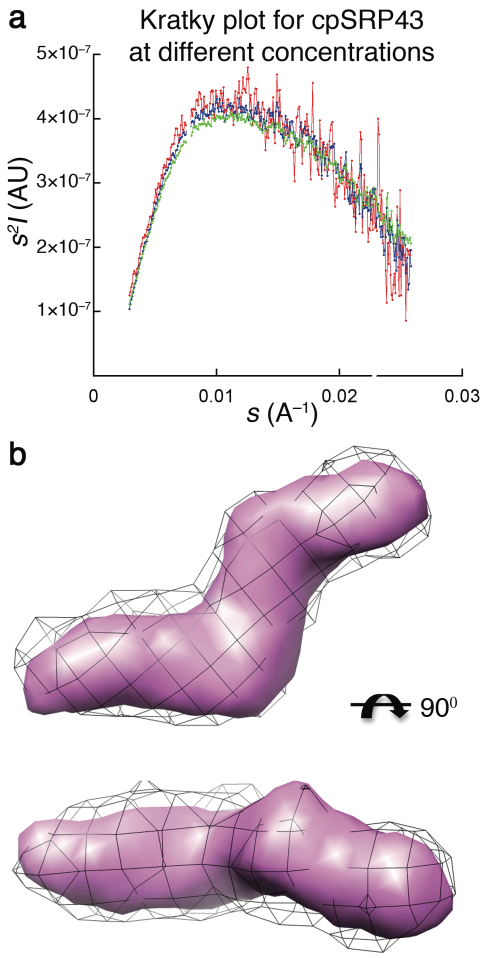

SAXS analysis of full-length cpSRP43. (a) Experimental SAXS profiles in Kratky's representation at cpSRP43 concentrations of 50 µM (red), 100 µM (blue), and 200 µM (green). The agreement of the three curves indicated that no aggregation or interparticle interference occurred during the experiment. **(b)** Comparison of surface maps calculated from the dummy atom model in Figure 8b (pink shell) and from the docking model in Figure 8c (gray mesh).

Supplementary Figure 7

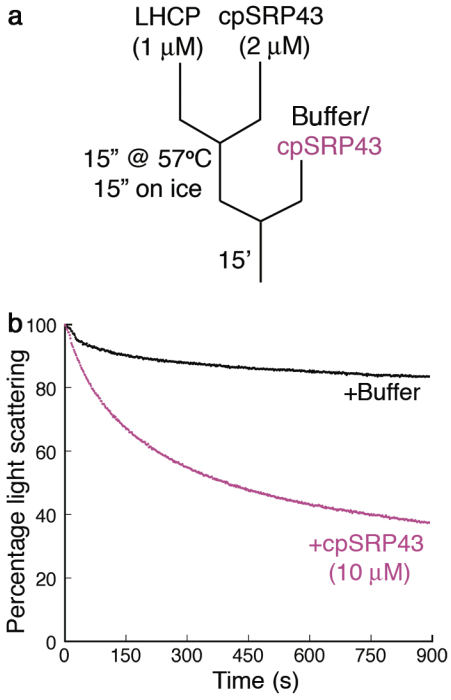

cpSRP43 can reverse heat-denatured LHCP aggregates. (**a**) Reaction scheme of the disaggregation assay using LHCP aggregates generated by heating the soluble LHCP–cpSRP43 complex. (**b**) Time courses for disaggregation reactions in the absence (black) and presence (magenta) of fresh cpSRP43 added after heat-induced aggregation of LHCP.

Supplementary Table 1 Comparison of disaggregation rate constants obtained from fits of data and simulation.

[cpSRP43] (μM)	k_f from manual fits of data (s^{-1})	k_3 from simulation (s^{-1})
2	0.0018	0.0023
4	0.0034	0.0041
6	0.0036	0.0050
8	0.0084	0.0084
10	0.0187	0.0180

Supplementary Note

Optimization of conditions for reconstituting the LHCP-cpSRP interaction.

Previous work suggested that both the cpSRP43 and cpSRP54 subunits are necessary for the formation of a soluble 'transit complex' with LHCP[12]. Our results here strongly suggested that cpSRP43 is sufficient to bind and solubilize LHCP. The disparity between this and the previous studies could stem, in part, from the differences in experimental conditions. We have found that the activity and oligomeric state of cpSRP43 is sensitive to ionic strength. In buffers with low ionic strength (<100 mM NaCl), which was typically used in previous studies, cpSRP43 exists as higher molecular weight complexes (Supplementary Fig. 1a). Under these low-salt conditions, cpSRP43 was sub-optimal for interacting with LHCP (Supplementary Fig. 1b,c). Presumably, the presence of cpSRP54 shifted the conformational equilibrium of cpSRP43 toward the more active monomeric state, and this likely contributed to the apparent requirement of cpSRP54 for interacting with LHCP under the previous assay conditions.

Kinetic simulations.

The Berkeley Madonna software was used to perform kinetic simulations for the different models of LHCP disaggregation (Fig. 4c,d). For the passive model in Figure 4c, the following reactions were modeled (eq. 1-2):

$$\mathrm{LHCP_{agg}} \underset{k_{-1}}{\overset{k_1}{\rightleftharpoons}} \mathrm{LHCP} \qquad (1)$$

$$\mathrm{LHCP} \underset{k_{-2}}{\overset{k_2}{\rightleftharpoons}} \mathrm{LHCP_{cmplx}} \qquad (2)$$

For the active mechanism in Figure 4d, the following reactions were modeled (eq. 1-3):

$$LHCP_{agg} \underset{k_{-1}}{\overset{k_1}{\rightleftharpoons}} LHCP \quad (1)$$

$$LHCP \underset{k_{-2}}{\overset{k_2}{\rightleftharpoons}} LHCP_{cmplx} \quad (2)$$

$$LHCP_{agg} \underset{k_{-3}}{\overset{k_3}{\rightleftharpoons}} LHCP_{cmplx} \quad (3)$$

in which $LHCP_{agg}$ denotes the aggregated LHCP molecules, LHCP denotes a soluble LHCP monomer, $LHCP_{cmplx}$ denotes the cpSRP43-LHCP complex, and the rate constants are defined in Figs 3c and d. As this software considers only first-order or pseudo-first-order reactions, the concentration of cpSRP43 was varied by varying the values of k_2 and k_3 during the simulation. For the aggregation reaction (eq. 1), the rate constant for LHCP aggregation (k_{-1}) was estimated to be 0.05 s^{-1}, based on the observation that LHCP aggregation is 70–80% complete within the first 15–20 seconds of mixing (Fig. 1c, 4e, and Supplementary Figs. 3, 5). As the light scattering from aggregates was linear with LHCP concentration starting from 0.5 μM (Fig. 1c) indicating complete aggregate formation above this concentration, we assumed that the equilibrium favors aggregation by 100-fold under the experimental conditions. This gave the apparent rate of spontaneous disaggregation (k_1) of 0.0005 s^{-1}; changing the value of k_1 from 0.00005 to 0.05 s^{-1} altered the time courses, but did not affect the conclusion that the disaggregation rates are independent of cpSRP43 concentrations in the passive mechanism (Supplementary Fig. 2).

For the binding reaction between LHCP monomer and cpSRP43 (eq. 2), we assumed an association rate constant (k_{on}) of 1×10^6 $M^{-1}s^{-1}$, which is typical for bimolecular association between proteins. Varying the value of k_{on} from 10^6 to 10^8

$M^{-1}s^{-1}$ had no effect on the result of simulation (not shown). The value of k_{on} and the experimentally determined K_d value of ~100 nM (Fig. 2a) were used to calculate the dissociation rate constant (k_{-2}). The apparent associating rate constants, k_2, were calculated as $k_{on} \times$ [cpSRP43].

For the active disaggregation reaction (eq. 3), we allowed the simulation program to fit the k_3 and k_{-3} values using experimental data. The values obtained from the simulation are comparable to the rate constants of disaggregation obtained from manual fitting of data (Supplementary Table 1; see the next section).

Analysis of rate constants for protein disaggregation.

The rate constants of protein disaggregation were obtained using several independent approaches. (i) The time course of LHCP disaggregation in Figure 4e were fit to equation 1 in Methods to obtain the observed rate constants to reach equilibrium (k_{obsd}), which is the sum of forward disaggregation and reverse re-aggregation processes ($k_{obsd} = k_f + k_r$), and the equilibrium of each disaggregation reaction, which is determined by the relative magnitude of the disaggregation and re-aggregation processes [$K_{obsd} = k_f/(k_f + k_r)$]. Using these relationships, we calculated the net rate constants for the disaggregation process (k_f). (ii) In cases where a substantial amount of disaggregation was achieved, the rate constants for the forward disaggregation reactions can also be estimated from the initial rates, since at earlier times the contribution from the reverse re-aggregation process is negligible. (iii) The Berkeley-Madonna program was used to fit the data in Figure 4e to the active remodeling mechanism in Figure 4d. The rate

constants obtained from these different approaches were the same, within experimental error (Supplementary Table 1).